Comparison of Three Tissue Composition Measurement Techniques Using Digital Mammograms— A Signal-to-Noise Study

Darryl S. Breitenstein and Chris C. Shaw

Tissue composition measurement may provide a quantitatively and physically meaningful method to objectively determine the "mammographic density" linked to breast cancer risk. A single energy hybrid (SEH) technique is described for measuring the tissue composition on a pixel-by-pixel basis with a single digital mammogram. Theoretical models were derived and used to compute signal-to-noise ratios (SNRs) in tissue composition measurement using the SEH method. The results were compared with those computed for measurements using the dual kVp and dual screen methods. SNRs were theoretically related to the pixel area, total unattenuated detector exposure and fluence spectra of the incident X-rays. SNRs were computed for measurement of the adipose tissue thickness for a 6 cm thick breast, consisting of 50% of adipose tissue and 50% of glandular tissue. Effects of kVp and prepatient filtration were studied by computing the SNRs for various kVps and filters and optimal kVps and filters are determined. The results showed that the SNRs obtained with the SEH method is an order of magnitude better than the dual kVp method, which, in turn, is an order of magnitude better than the dual screen method. When using the optimal kVp's and no prepatient filtration, the SNRs were computed to be 84.2, 13.2, and 2.0 for the SEH, dual kVp, and dual screen methods, respectively. Prepatient filtration can improve the SNR by as much as 35% for the dual kVp and dual screen techniques with reasonable tube loading factors (8-10).

KEY WORDS: computed radiography (CR), digital mammography, numerical simulation, optimization, tissue composition measurement, signal-to-noise ratio.

BREAST TISSUE can be divided into the following two types: adipose (fat) and glandular. Because mammograms are generally acquired with breasts compressed to uniform thickness (except along the border), tissue composition and its spatial variation dictate the production of radiographic density and image structures in mammograms.[1,2] In addition to diagnosis, radiographic density and image structures can also be used to qualitatively estimate the "density" of the breast imaged, which refers to the relative amount of fibroglandular tissue present in the breast. This density is often referred to as the "mammographic density" and has been extensively investigated as a factor that can be linked to breast cancer risk.[3-8] It has been reported that mammographically dense breasts have a risk factor several times higher than those not considered as such. Although the factor of increase reported on have varied, they were all quite significant. It has been proposed that mammographic density can be used to identify women at high-risk and to alter the strategy of screening accordingly for early detection of breast cancer.

Despite the success of many studies in identifying the mammographic density as a factor or indicator for breast cancer risk, the determination of mammographic density has varied greatly in its methodology in different studies.[6] Early studies rely on completely subjective classification of mammograms into several categories with different degrees of mammographic density. More recently, there have been studies with digitized mammograms and threshold film density display method to determine the mammographic density in a semi-quantitative way.[3,8] Despite the efforts of developing and using computerized methods to improve the consistency and reproducibility, there has been no attempt to directly convert mammographic image information into composition and distribution of fibroglandular tissue in the breast for more quantitative and accurate determination of the mammographic density. Such approach would re-

From the Naval Surface Warfare Center, Dahlgren Division, Dahlgren, VA; and the Department of Radiology, University of Pittsburgh, Pittsburgh, PA.

This work was supported in part by a grant (CA 51248) from the National Cancer Institute, a grant (DAMD 17-93-J-3009) from the U.S. Army Medical Research and Material Command, a grant (DAAH 04-93-G-0299) from the Department of Defense, and a grant, "Breast Fat Measurement," from the Pittsburgh Cancer Institute.

Address reprint requests to Chris C. Shaw, PhD, A439 Scaife Hall, Department of Radiology, University of Pittsburgh, Pittsburgh, PA 15261.

0897-1889/98/1103-0005$8.00/0

quire the tissue composition or ratio of fibroglandular tissue to be measured on a pixel-by-pixel basis in a mammogram. It has the advantage of providing a physically meaningful and universal standard in defining and determining the mammographic density.

Tissue composition measurement can best be developed with digital mammography systems, providing high-quality digital image data facilitating the implementation of necessary image processing and analysis schemes for such measurement. A variety of different digital mammography techniques have been developed, investigated, and even commercialized.[9-14] They are based on new detector technologies, including the charge-coupled-device (CCD), amorphous silicon flat panel detector, CsI screens, or storage phosphors. As these systems become available for clinical use, it becomes feasible to process the mammographic image information and convert them into tissue composition measurement on a pixel-by-pixel basis for determining and studying the mammographic density.

Dual-energy subtraction techniques have long been used to separate image signals into components corresponding to two or even three attenuating materials.[15-24] The applications include bone mineral measurement, dual-energy chest radiography, dual-energy mammography, and tissue composition measurement. Two major approaches have been developed over the years to implement the dual-energy subtraction imaging or measurement techniques.[15,16,25-28] The dual-kVp technique requires two radiograph images to be acquired with two separate exposures made with different kVp's and filtration schemes.[27] The single exposure technique employs two image detectors with or without an interdetector filter to simultaneously acquire low- and high-energy image for dual-energy subtraction processing. This technique has been investigated and commercialized for use in computed radiography (CR) chest imaging to separate the tissue and bone structures.

Mammographic imaging differs from other imaging applications in that the breast is generally well compressed to have a largely uniform thickness. By directly measuring the total breast thickness, the adipose and glandular tissue thicknesses are no longer independent of each other. The typical problem of measuring two component thicknesses is reduced to that of measuring only one because knowing one, the other can be easily calculated. As the result, a single X-ray measurement is needed to determine the tissue composition. In this article, we describe and study the technique of using a single mammogram in conjunction with proper calibration to measure tissue composition on a pixel-by-pixel basis. Because one, instead of two, X-ray measurement was used, this method, referred to as the single energy hybrid (SEH) method, is expected to produce less noisy measurement. In this article, the noise properties of the SEH measurement are studied and compared with the dual-kVp and dual-screen methods. Theoretical modeling and numerical computation were used to estimate the SNRs for measuring the adipose tissue thickness for 6 cm thick 50% adipose and 50% glandular breast tissue. Effects of kVp and prepatient filtration were also computed. The results are presented and compared to those computed for the dual-kVp and dual-screen methods.

THEORY

Breasts can be considered as composed of two basic types of tissue: the adipose or fat tissue and the glandular tissue. Atomic composition and X-ray attenuation properties have been previously investigated and reported on.[29] In the general sense, tissue composition measurement for the breast requires the measurement of both the adipose and glandular tissue thicknesses. However, mammographic imaging differs from other radiographic procedures in that the breast is compressed to a largely uniform total thickness that can be easily measured. Thus, the task of tissue composition measurement (through radiograph imaging procedure) is reduced to that of measuring the thickness for one (eg, adipose) of the two types of tissues because the adipose and glandular tissue thicknesses are no longer independent of each other. This forms the basis for the SEH method to be described and discussed later. The dual-energy method, on the hand, does not take the advantage of breast compression. Instead, it is capable of measuring both adipose and glandular tissue thicknesses without requiring the total breast thickness to be fixed and known.

Despite the potential benefit of obtaining diagnostic information in a radiograph imaging or mea-

surement procedure, the patient is also subject to risk of damage by ionizing radiation. Thus, the benefits of all radiograph imaging or measurement procedures should be evaluated and weighed against a fixed risk to the patient. Whereas the benefits and risk of these procedures are often only known partially or in a qualitative manner, they can be indirectly quantified by the quality of the resulting image or measurement and exposure to the patient, respectively. The quality of the tissue composition measurement can be quantified by the precision or SNR of the adipose tissue thickness measured. The risk of the measurement, on the other hand, can be quantified by the radiation exposure to the patient. Although the skin entrance exposure or midbreast exposure is often used to quantify the radiation risk in mammographic procedures, it is adequate here to compute and compare the SNR of adipose tissue thickness measurement for a fixed total unattenuated (in the absence of the breast) exposure to the X-ray detector. For a fixed imaging geometry, this normalizes the patient risk in the comparison study. In this section, a theoretical model will be derived to relate the noise variance of the adipose tissue thickness measurement to the unattenuated detector exposure under various imaging conditions. This model allows the noise variance to be computed using published data for X-ray spectra and attenuation coefficients.

Single Energy Hybrid Method

With a well compressed breast, the total breast thickness can be assumed to be uniform and known. The SEH method employs calibration measurements to compute a lookup table, which can then be used to map digital mammogram image data into tissue composition. This method can be illustrated by a schematic drawing shown in Fig 1.

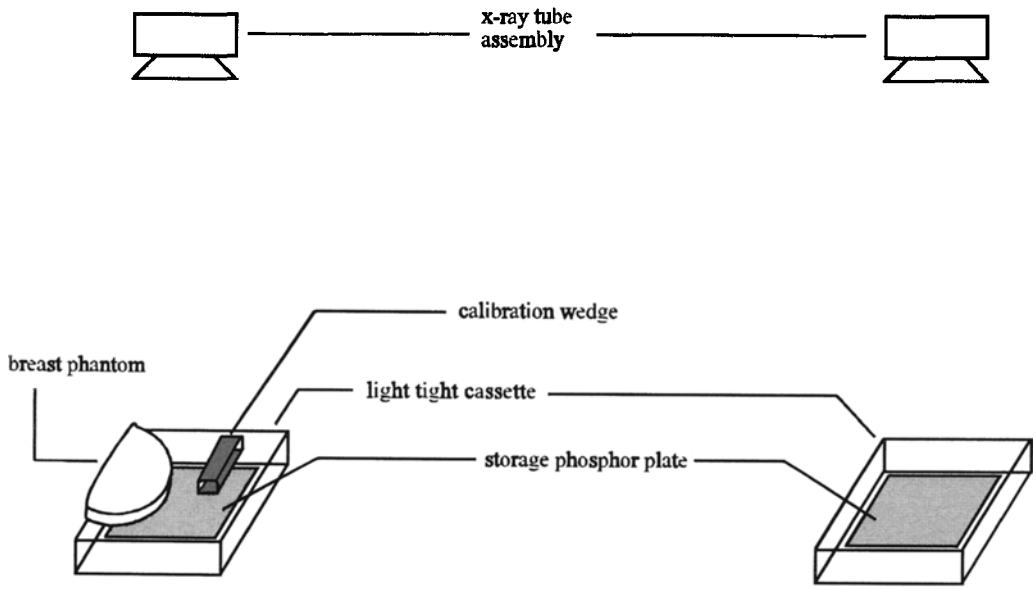

$$D = \ln\left(\frac{p^o}{p}\right)$$

$$t_a = f_a(D)$$

Fig 1. Schematic drawing for the single energy hybrid (SEH) method for tissue composition measurements. A open field image and an image of calibration phantom are required to provide reference and information for constructing the lookup table to convert the image signals into tissue composition measurement.

Neglecting X-ray and light scattering, the image signal for a specific pixel, p, can be expressed as:

$$p = \int AR\phi(E)e^{(-\mu_a(E)t_a-\mu_g(E)t_g)}S(E)Q(E)\,dE \quad (1)$$

where A is the area of the pixel in cm^2; R is the unattenuated X-ray exposure (in milliroentgens); E is the photon energy in keV; $\phi(E)$ is the energy dependent photon fluence per unit exposure and photon energy (photons/cm^2 mR keV); S(E) is the X-ray absorption ratio for the detector; Q(E) is the average signal gain per X-ray photon of energy E; $\mu_a(E)$ and $\mu_g(E)$ are the energy dependent linear attenuation coefficients (in cm^{-1}) for adipose and glandular tissues, respectively; and t_a and t_g are the thicknesses in cm of the adipose and glandular tissues. Since the X-ray field is not uniform, a reference image, p^0, acquired without the breast present, is required and can be express as:

$$p^0 = \int AR\phi(E)S(E)Q(E)\,dE \quad (2)$$

A quantity referred to as the X-ray density, D, can be defined as the natural logarithm of p^0/p, and used to relate image signals to the attenuating materials in a way independent of the intensity variation of incident X-rays. As defined, D can be expressed as:

$$\begin{aligned} D &= \ln\left(\frac{p^0}{p}\right) \\ &= \ln\left(\frac{\int AR\phi(E)S(E)Q(E)\,dE}{\int AR\phi(E)S(E)e^{(-\mu_a(E)t_a-\mu_g(E)t_g)}\cdot Q(E)\,dE}\right) \\ &= \ln\left(\frac{\int AR\phi(E)S(E)Q(E)\,dE}{\int AR\phi(E)S(E)e^{(-\mu_a(E)t_a-\mu_g(E)(t-t_a))}\cdot Q(E)\,dE}\right) \end{aligned} \quad (3)$$

In the SEH measurement, the X-ray density, D, computed from the digital mammogram and the reference signal is a function of and can be mapped to the adipose thickness, t_a. Thus, the noise variance in the measurement of t_a, $\sigma^2_{t_a}$, can be related to the noise variance in D, σ^2_D as follows:

$$\sigma^2_{t_a} = \frac{\sigma^2_D}{\left(\frac{\partial D}{\partial t_a}\right)^2} \quad (4)$$

Thus, to estimate $\sigma^2_{t_a}$, it is necessary to evaluate σ^2_D and $\partial D/\partial t_a$. σ^2_D can be related to p and its noise variance, σ^2_p, as follows:

$$\begin{aligned} \sigma^2_D &= \left(\frac{\partial D}{\partial p}\right)^2\sigma^2_p + \left(\frac{\partial D}{\partial p_0}\right)^2\sigma^2_{p_0} \\ &= \left(\frac{\partial\left(\ln\left(\frac{p^0}{p}\right)\right)}{\partial p}\right)^2\sigma^2_p + \left(\frac{\partial\left(\ln\left(\frac{p^0}{p}\right)\right)}{\partial p_0}\right)^2\sigma^2_{p_0} \\ &= \frac{\sigma^2_p}{p^2} + \frac{\sigma^2_{p_0}}{p_0^2} \\ &\approx \frac{1}{SNR^2_p} \end{aligned} \quad (5)$$

where $SNR_p = p/\sigma_p$ and it is assumed that the reference signal, p^0, has a high SNR and therefore negligible contribution to σ^2_D. This assumption is valid because p^0 is produced from unattenuated X-rays consisting of a much larger number of detected photons than the attenuated signal, p. To determine SNR_p, the noise fluctuation of the image signal, p, is assumed to originate from X-ray detection only and σ^2_p may be calculated by integrating the noise variances in each energy interval as follows:

$$\sigma^2_p = \int AR\phi(E)e^{(-\mu_a(E)t_a-\mu_g(E)t_g)}S(E)Q^2(E)\,dE \quad (6)$$

where $AR\phi(E)e^{(-\mu_a(E)t_a-\mu_g(E)t_g)}S(E)dE$ is the number of detected photons in the energy interval between E and E + dE, which is multiplied with $Q(E)^2$ to convert noise variances of detected number of photons into those of image signals. Combining Eqs. 1 and 6, SNR_p can be computed as follows:

$$\begin{aligned} SNR^2_p &= \frac{p^2}{\sigma^2_p} \\ &= \frac{\left[\int AR\phi(E)e^{(-\mu_a(E)t_a-\mu_g(E)t_g)}\cdot S(E)Q(E)\,dE\right]^2}{\int AR\phi(E)e^{(-\mu_a(E)t_a-\mu_g(E)t_g)}S(E)Q^2(E)\,dE} \\ &= \frac{AR\left[\int AR\phi(E)\,e^{(-\mu_a(E)t_a-\mu_g(E)t_g)}\cdot S(E)Q(E)\,dE\right]^2}{\int \phi(E)e^{(-\mu_a(E)t_a-\mu_g(E)t_g)}\cdot S(E)Q^2(E)\,dE} \end{aligned} \quad (7)$$

Thus, SNR_p^2 is proportional to the pixel area and the unattenuated detector exposure. Equation 7 can be further simplified by assuming that $Q(E) = \alpha E$:[30]

$$SNR_p^2 = \frac{AR\left[\int \phi(E)e^{(-\mu_a(E)t_a - \mu_g(E)t_g)}S(E)E\,dE\right]^2}{\int \phi(E)e^{(-\mu_a(E)t_a - \mu_g(E)t_g)}S(E)E^2\,dE} \quad (8)$$

Using equation 3, $\partial D/\partial t_a$ can be evaluated and expressed as follows:

$$\begin{aligned}
\frac{\partial D}{\partial t_a} &= \frac{\partial\left(\ln\left(\frac{p^0}{p}\right)\right)}{\partial t_a} \\
&= -\frac{1}{p}\frac{\partial\left(\int AR\phi(E)S(E)e^{(-\mu_a(E)t_a - \mu_g(E)t_g)}Q(E)\,dE\right)}{\partial t_a} \\
&= -\frac{1}{p}\frac{\partial\left(\int AR\phi(E)S(E)e^{(-\mu_a(E)t_a - \mu_g(E)(t-t_g))}Q(E)\,dE\right)}{\partial t_a} \\
&= \frac{\int AR\phi(E)S(E)(\mu_a(E) - \mu_g(E))e^{(-\mu_a(E)t_a - \mu_g(E)t_g)}Q(E)\,dE}{\int AR\phi(E)S(E)e^{(-\mu_a(E)t_a - \mu_g(E)t_g)}Q(E)\,dE} \\
&= \frac{\int (\mu_a(E) - \mu_g(E))AR\phi(E)S(E)e^{(-\mu_a(E)t_a - \mu_g(E)(t-t_a))}Q(E)\,dE}{\int AR\phi(E)S(E)e^{(-\mu_a(E)t_a - \mu_g(E)(t-t_a))}Q(E)\,dE} \\
&= \frac{\int (\mu_a(E) - \mu_g(E))AR\phi(E)S(E)e^{(-\mu_a(E)t_a - \mu_g(E)t_g)}Q(E)\,dE}{\int AR\phi(E)S(E)e^{(-\mu_a(E)t_a - \mu_g(E)t_g)}Q(E)\,dE} \\
&= \langle\Delta\mu(E)\rangle|_p
\end{aligned} \quad (9)$$

Equation 9 shows that $\partial D/\partial t_a$ is the difference in attenuation coefficients, $\Delta\mu(E) = \mu_a(E) - \mu_g(E))$, averaged over the energy spectrum of the image signal and therefore denoted by $\langle\Delta\mu\rangle|_p$. Assuming that $Q(E) = \alpha E$:

$$\langle\Delta\mu(E)\rangle|_p = \frac{\int (\mu_a(E) - \mu_g(E))\phi(E)S(E) \cdot e^{(-\mu_a(E)t_a - \mu_g(E)t_g)}E\,dE}{\int \phi(E)S(E)e^{(-\mu_a(E)t_a - \mu_g(E)t_g)}E\,dE} \quad (10)$$

By using equations 8 and 10, $\sigma_{t_a}^2$ can be estimated as follows:

$$\sigma_{t_a}^2 = \frac{1}{\langle\Delta\mu\rangle|_p^2} \cdot \frac{1}{SNR_p^2} \quad (11)$$

This equation indicates that the noise variance in measuring the adipose tissue thickness is inversely proportional to the SNR of the image signal and to the average difference in the attenuation coefficients for the adipose and glandular tissues. Because $\langle\Delta\mu\rangle|_p$ is independent of the pixel area and unattenuated detector exposure, as shown by equation 10, $\sigma_{t_a}^2$ is inversely proportional to the pixel area and the unattenuated detector exposure.

Dual Energy Methods

The dual energy method requires the use of a low energy X-rays image and a high energy X-rays image to obtain thickness measurements for the two different attenuating materials: adipose and glandular tissues. This method is sometimes referred to as dual-energy subtraction imaging technique because it is used in some applications to cancel out background attenuating material structures enhancing the visualization of the other attenuating material structure. In contrast to the SEH method, the dual-energy methods do not require the total breast thickness to be fixed or known. It can be used to measure an arbitrary combination of adipose and glandular tissue thicknesses. Another way to look at this feature is that it can be used to measure both the total breast

thickness and the tissue composition even if the former varies from pixel to pixel. Depending on how low- and high-energy images are obtained, there are several different approaches to dual-energy measurements. A theoretical model for tissue and bone thickness measurement in chest imaging has been previously derived and used to compute the SNRs for soft-tissue and bone thickness signals. This model can be applied to tissue composition measurement in mammographic imaging with little modification.

With the dual-energy method, the adipose and glandular tissue thicknesses, t_a and t_g, can be represented as functions of the X-ray densities computed from low- and high-energy images, D_l and D_h, as follows:

$$t_{a,g} = f_{a,g}(D_l, D_h) \tag{12}$$

where D_l and D_h are the low and high energy x-ray densities defined as follows:

$$D_{l,h} = \ln\left(\frac{p^0_{l,h}}{p_{l,h}}\right) \tag{13}$$

where p_l and p_l^0 represent the attenuated and nonattenuated image signals from the low-energy spectrum, and p_h and p_h^0 represent the corresponding signals from the high-energy spectrum. Neglecting X-ray or light scattering, $p^0_{l,h}$ and $p_{l,h}$ may be expressed as:

$$p^0_{l,h} = \int AR_{l,h}\phi_{l,h}(E)S(E)Q(E)\,dE \tag{14}$$

and

$$p_{l,h} = \int AR_{l,h}\phi_{l,h}(E)e^{-\mu_a(E)t_a-\mu_g(E)t_g} \cdot S(E)Q(E)\,dE \tag{15}$$

where A is the pixel area; S(E) is the X-ray absorption ratio for the detector; $R_{l,h}$ are the unattenuated X-ray exposures in mRs at the detector plane and $\phi_{l,h}(E)$ are the unattenuated photon fluence per unit exposure per unit energy (photons/cm^2 mR keV) for low- and high-energy X-rays, respectively; Q(E) is the detector response function; $\mu_{a,g}(E)$ are the linear attenuation coefficient for adipose and glandular tissues, respectively.

As previously derived, the noise variances of the component thickness measurements (t_a and t_g in this study), $\sigma^2_{t_a}$ and $\sigma^2_{t_g}$ can be computed as follows[28]:

$$\sigma^2_{t_a} = \frac{k^2_{al}}{SNR^2_{p_l}} + \frac{k^2_{ah}}{SNR^2_{p_h}} \tag{16}$$

$$\sigma^2_{t_g} = \frac{k^2_{gl}}{SNR^2_{p_l}} + \frac{k^2_{gh}}{SNR^2_{p_h}} \tag{17}$$

where $SNR_{p_{l,g}}$ are the SNRs for p_l and p_h and the coefficients, k_{ij}'s, can be computed as the inverse matrix to the average attenuation coefficients, μ_{ij}'s, as follows:

$$\begin{bmatrix} k_{al} & k_{ah} \\ k_{gl} & k_{gh} \end{bmatrix} = \begin{bmatrix} \mu_{al} & \mu_{gl} \\ \mu_{ah} & \mu_{gh} \end{bmatrix}^{-1} \tag{18}$$

while μ_{ij}'s are computed as the attenuation coefficient for tissue i (i = a or g) averaged over the spectrum j (j = l or h) as follows:

$$\mu_{ij} = \left[\frac{\int \mu_i(E)AR_j\phi_j(E)e^{-\mu_a(E)t_a-\mu_g(E)t_g} S(E)Q(E)\,dE}{\int AR_j\phi_j(E)e^{-\mu_a(E)t_a-\mu_g(E)t_g} \cdot S(E)Q(E)\,dE}\right] = \langle\mu_i(E)\rangle|_{p_j} \tag{19}$$

Assuming that Q(E) = αE, equation 19 can be further simplified to be:

$$\mu_{ij} = \langle\mu_i(E)\rangle|_{p_j} = \left[\frac{\int \mu_i(E)\phi_j(E)e^{-\mu_a(E)t_a-\mu_g(E)t_g}S(E)E\,dE}{\int \phi_j(E)e^{-\mu_a(E)t_a-\mu_g(E)t_g}S(E)E\,dE}\right] \tag{20}$$

As in equation 8, $SNR^2_{p_{t,g}}$ in equations 16 and 17 and can be computed as follows:

$$SNR^2_{p_{l,h}} = \frac{AR\left[\int \phi_{l,h}(E)e^{(-\mu_a(E)t_a-\mu_g(E)t_g)} \cdot S(E)E\,dE\right]^2}{\int \phi_{l,h}(E)e^{(-\mu_a(E)t_a-\mu_g(E)t_g)} \cdot S(E)E^2\,dE} \tag{21}$$

Because μ_{ij}'s are independent of AR while $SNR^2_{p_{l,h}}$ are proportional to AR, the thickness variances are inversely proportional to A and R.

Generation of Dual-Energy X-rays

Depending on how dual-energy X-ray images are acquired, there are several different approaches to dual-energy measurement. One commonly used technique is the dual-kVp technique with low- and

high-energy images acquired by separate exposures using two different kVp's. Prepatient filters may also be used to enhance the spectral difference between low- and high-energy X-rays. With this technique, $\phi_l(E)$ and $\phi_h(E)$ are independent of each other and are given by the filtered spectra at low- and high-kVps, respectively. Notice that because each image requires a separate exposure, the total allowable exposure must be split between the two images.

A second technique is the dual-screen technique where two detectors (typically storage phosphor screens) are simultaneously exposed to acquire a front screen image and a back screen image. In this case, the X-rays incident to the front detector are the low-energy X-rays, characterized by the fluence, $\phi_l(E)$. Those incident to the back detector are the high-energy X-rays, as characterized by the fluence, $\phi_h(E)$, because they are filtered and hardened by the front detector as follows:

$$\phi_h(E) = (1 - S(E))\phi_l(E) \qquad (22)$$

With the dual-screen technique, $\phi_l(E)$ and $\phi_h(E)$ are not independent of each other and their difference is somewhat limited. However, because both $\phi_l(E)$ and $\phi_h(E)$ are generated with the same exposure, the full total allowable exposure can be used to acquire the images.

METHOD

For numerical computations all attenuation coefficients and X-ray spectra were obtained and interpolated from published data.[29,31-33] The detector is assumed to be one or two (for dual-screen technique) high-resolution storage phosphor image plates (Fuji HRIIIN) whose absorption ratio was obtained from the manufacturer's technical manual.[34] The pixel size was assumed to be 1 mm. Notice that this is the pixel size for measuring tissue compositions and it determines the spatial resolution at which the variation of tissue composition can be measured. The 1 mm pixel size is more than adequate for measuring and studying the variation of tissue composition. It should not be confused with the pixel size for actual images, which is often much smaller (as low as 43 μm) to allow microcalcifications to be rendered and visualized. The total allowable exposure was set to be 100 mR. This was assumed to be used in whole for the SEH and dual-screen technique but was split in half between low- and high-kVp exposures for the dual-kVp technique.

The SNRs were computed for the adipose tissue signal for a breast consisting of 3-cm thick adipose tissue and 3-cm thick glandular tissue for a total thickness of 6 cm. For the SEH method, equations 8, 10, and 11 were used to calculate the noise variance, $\sigma^2_{t_a}$, and the SNR, $SNR_{t_a} = t_a/\sigma_{t_a}$. SNRs were computed for mammographic X-ray spectra generated from a molybdenum target at 20 through 55 kVp, incremented by 5 kVp. The purpose of varying the kVp is to see if there is an optimal kVp for using this method. Examples of these spectra are shown in Figs 2 and 3.

Prepatient filtration may improve the SNR and was studied by computing the filtered spectrum as follows:

$$\phi_l(E) = k\, e^{-\mu_{filter}(E)t_{filter}}\phi_{unfiltered}(E) \qquad (23)$$

where $\mu_{filter}(E)$ and t_{filter} are the attenuation coefficient and thickness for the filter; $\phi_{unfiltered}(E)$ is the unfiltered spectrum interpolated from published data (normalized for unit exposure); and k is a constant to normalize $\phi_l(E)$ for unit exposure (mR). Because the filter was assumed to be placed between the X-ray tube and the breast, the computations were still normalized for 100 mR of unattenuated exposure at the detector. However, owing to filtration of X-rays, the mAs may have to be substantially increased. The normalization constant, k, which can also serve as the tube loading factor to measure how much the mAs setting must be increased, was computed as follows:

$$k = \frac{\int AR\phi_{unfiltered}(E)S(E)\alpha E\, dE}{\int AR\phi_{unfiltered}(E)e^{-\mu_{filter}(E)t_{filter}}S(E)\alpha E\, dE} = \frac{\int \phi_{unfiltered}(E)S(E)E\, dE}{\int \phi_{unfiltered}(E)e^{-\mu_{filter}(E)t_{filter}}S(E)E\, dE} \qquad (24)$$

For the dual-kVp method, equations 16, 18, 20, and 21 were used to compute the SNRs. The high-energy spectrum was fixed and chosen to be at 55 kVp. The low-energy spectrum was varied from 20 to 50 kVp, incremented by 5 kVp. The purpose of varying the kVp for the low-energy spectrum is to see if there is an optimal kVp when the high-energy spectrum is obtained at 55 kVp. Figure 3 shows the spectra for 25 and 55 kVp X-rays used in computations for the dual-kVp method. Improvement by prepatient filtration was studied by attenuating either the low- or high-kVp (not both) spectrum with aluminum or molybdenum of various thicknesses. The filtered spectrum and the normalization constant were computed in a similar way as for the SEH method. For all SNR computations, the 100 mR exposure was split between the low- and high-kVp spectrum. In support of this seemingly simplified approach, a SNR computation for the 25 to 55 kVp combination with various exposure distribution ratios was conducted to illustrate the effects of exposure distribution on the computed SNR.

For the dual-screen method, the same set of equations was used to compute the SNRs. However, $\phi_h(E)$ was computed from $\phi_l(E)$ through equation 22. The tube voltage of the incident X-rays was varied from 20 to 55 kVp, incremented by 5 kVp, to determine the optimal voltage for using the dual-screen method. Prepatient filtration of $\phi_l(E)$ was computed by using equation 23. Because $\phi_h(E)$ was essentially $\phi_l(E)$ filtered by the front detector, the filtration affects both $\phi_l(E)$ and $\phi_h(E)$.

RESULTS AND DISCUSSION

Single Energy Hybrid Method

The SNR computed for the SEH method is plotted as a function of the kVp in Fig 4. The SNRs range from 58 to 84.2, peaking at 30 kVp with the values for 25 kVp and 35 kVp slightly lower (83.0

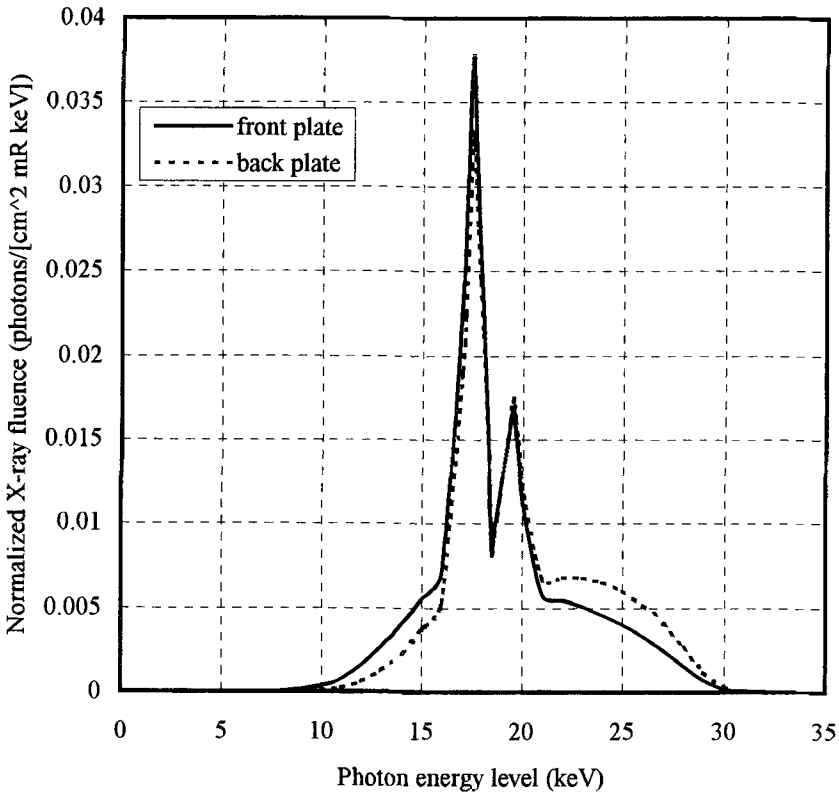

Fig 2. Detected X-ray spectra for the front and back image plates in dual screen measurement. The spectra were normalized for the same unattenuated exposure at the detector.

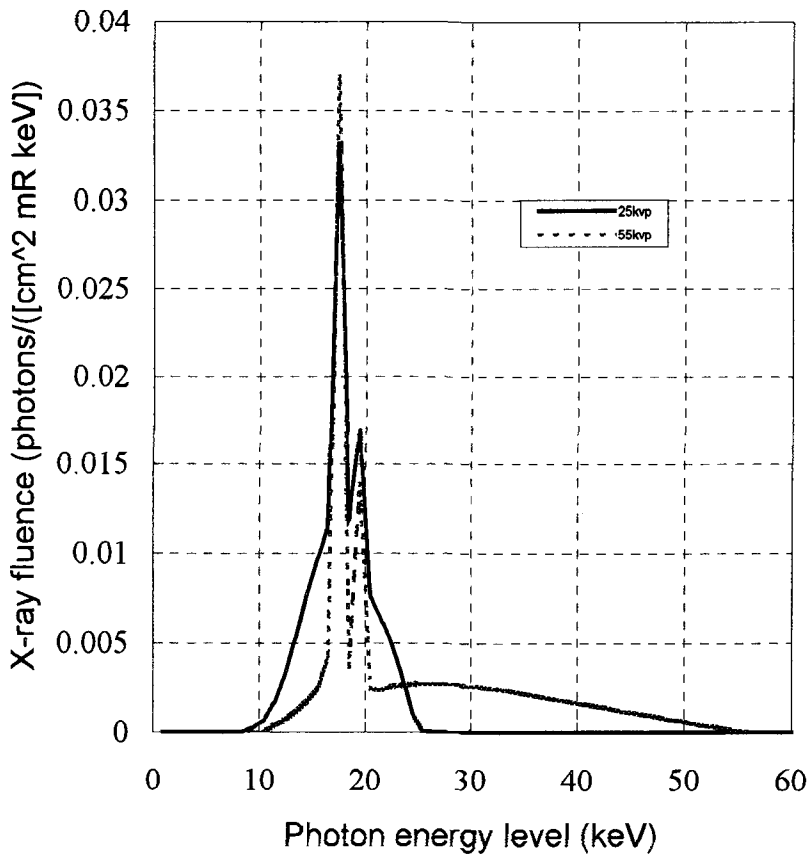

Fig 3. Detected X-ray spectra for 25 kVp and 55 kVp X-rays used in the dual kVp measurement. The spectra were normalized for the same unattenuated exposure at the detector.

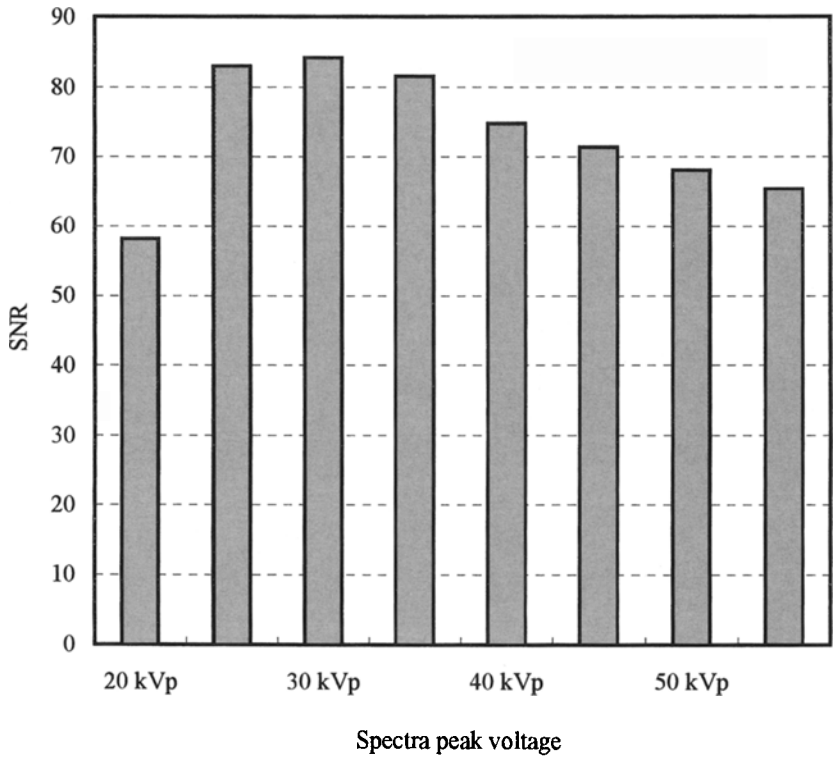

Fig 4. SNR computed for the SEH measurement versus X-ray tube voltage.

and 81.5, respectively). Prepatient filtration was found to improve the SNR. However, significant improvement can be obtained only at the expense of substantial heat loading to the X-ray tube. The tube loading factor is so large that SNR improvement with prepatient filtration is impractical.

Dual kVp Method

The SNRs computed for the dual-kVp method are plotted as a function of the kVp of the low-energy X-rays in Fig 5 (with the kVp of the high-energy X-rays kept at 55 kVp) and as a function of the kVp of the high-energy X-rays in Fig 6 (with the kVp of the low-energy X-rays kept at 20 kVp). Both plots indicate that it is generally advantageous to keep the kVps of the low- and high-energy X-rays as far apart from each other as possible. However, in Fig 5, the SNR actually peaks at 25 kVp and decreases slightly at 20 kVp. This may be explained by the fact that mammographic X-ray spectra generally take advantage of the characteristic X-rays at about 17 and 19 keV, producing good image contrast while maintaining sufficient penetration through the breast. When the kVp decreases towards 20 kVp, these characteristic X-rays decrease in weight in the spectrum and are replaced by X-rays of lower energies that do not penetrate the breast well and produce poor SNRs.

The dual kVp method differs from the SEH and dual screen methods by requiring two patient exposures versus only one. Thus, the total allowable exposure must be distributed between the low- and high-kVp images. To study the impact of exposure distribution on the SNRs, the SNR was computed for various low kVp exposure ratios, defined as the ratios of low kVp exposure to the total exposure, by using the combination of 25 and 55 kVp X-rays. In Fig 7, the computed SNR is plotted as a function of the low kVp exposure ratio. The plot shows that the SNR peaks at 50% with those at 40% and 60% slightly lower (<3%). This shows that the choice of 50%-to-50% exposure distribution is reasonably close to the optimal one.

In Fig 8, the SNRs, computed for 25 and 55 kVp X-rays, are plotted as the function of the filter thickness for four different filtration methods. The plots show that filtration of the high kVp spectrum by aluminum produces the best results. With 1 mm thick aluminum filter, it can increase the SNR by almost 30% (from 13.2 to 17.8) with a tube loading factor of only 7.65. The plots show that filtration of the low kVp X-rays by aluminum does not result in

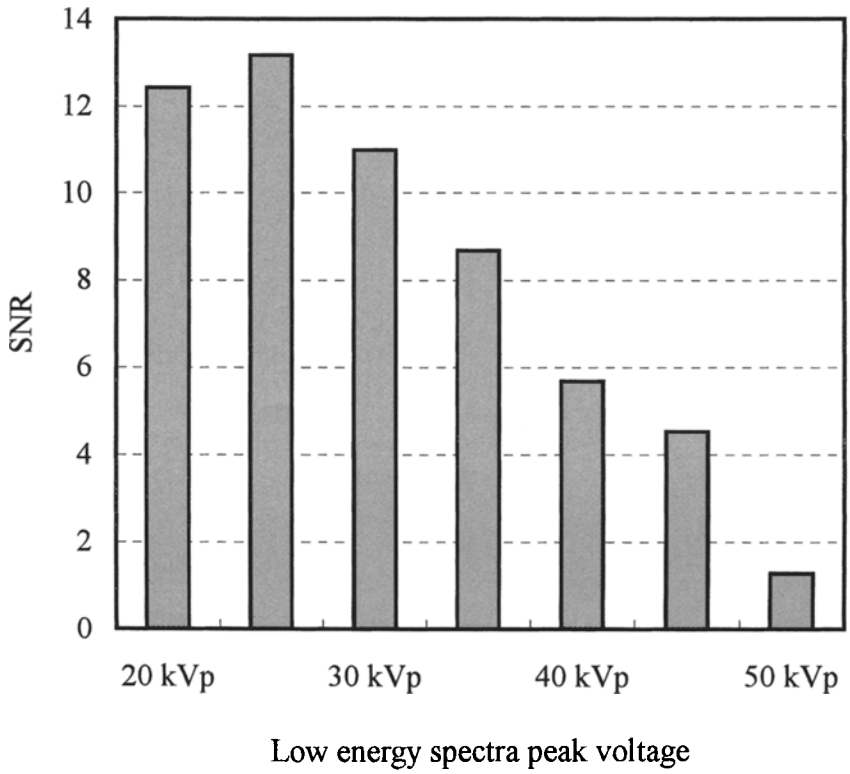

Fig 5. SNR computed for the dual kVp measurement versus low-energy X-ray tube voltage. The high energy tube voltage was kept fixed at 55 kVp.

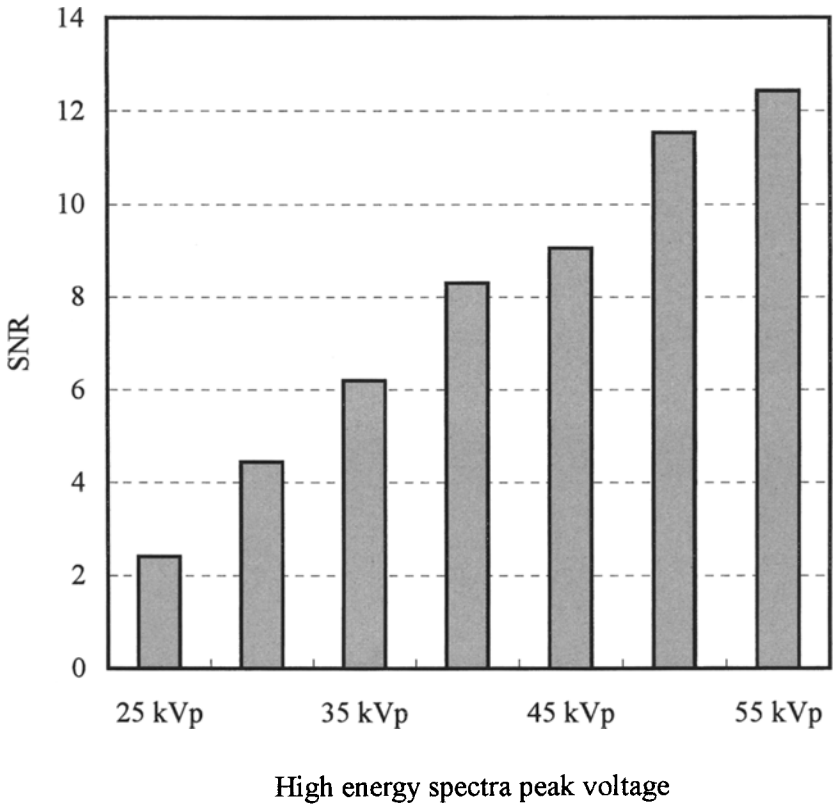

Fig 6. SNR computed for the dual kVp measurement versus high-energy X-ray tube voltage. The low-energy tube voltage was kept fixed at 20 kVp.

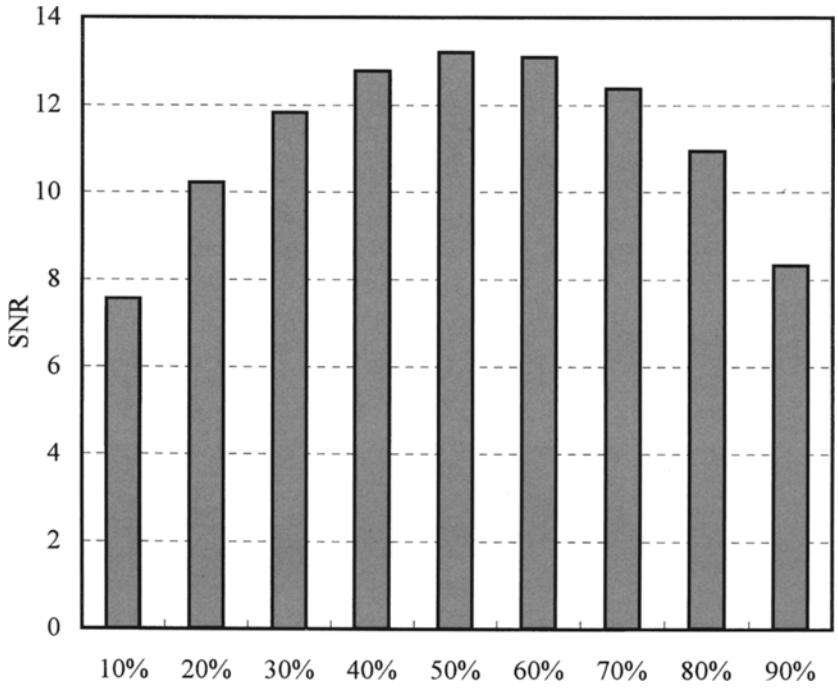

Fig 7. SNR versus ratio of low-kVp exposure in the dual kVp measurement with 25 and 55 kVp X-rays.

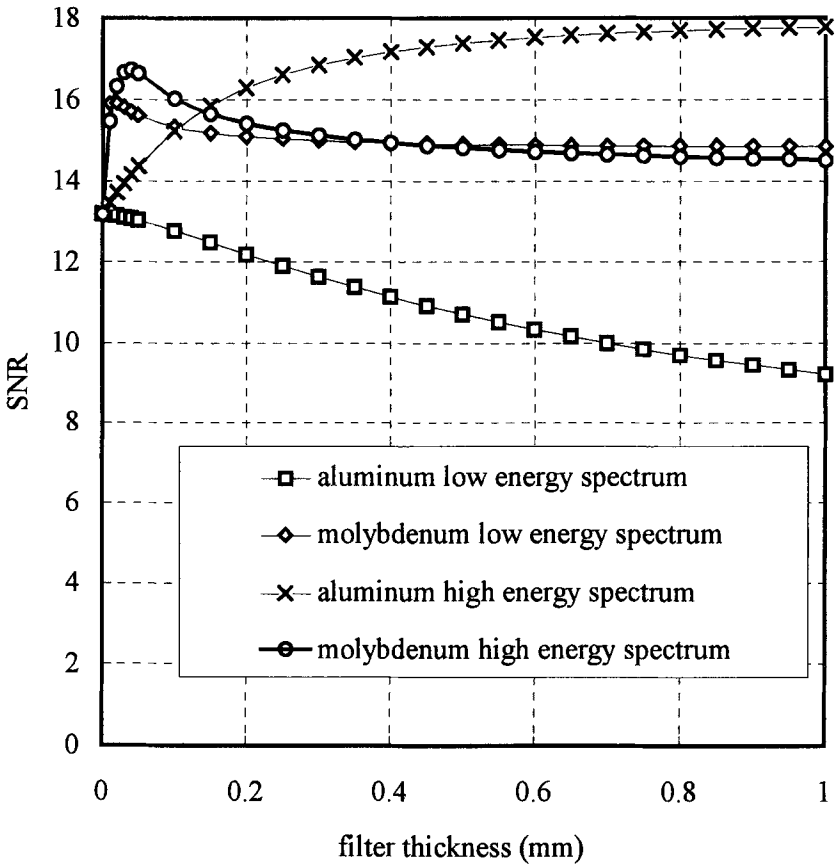

Fig 8. SNR versus filter thickness for four different schemes of prepatient filtration in dual kVp measurement.

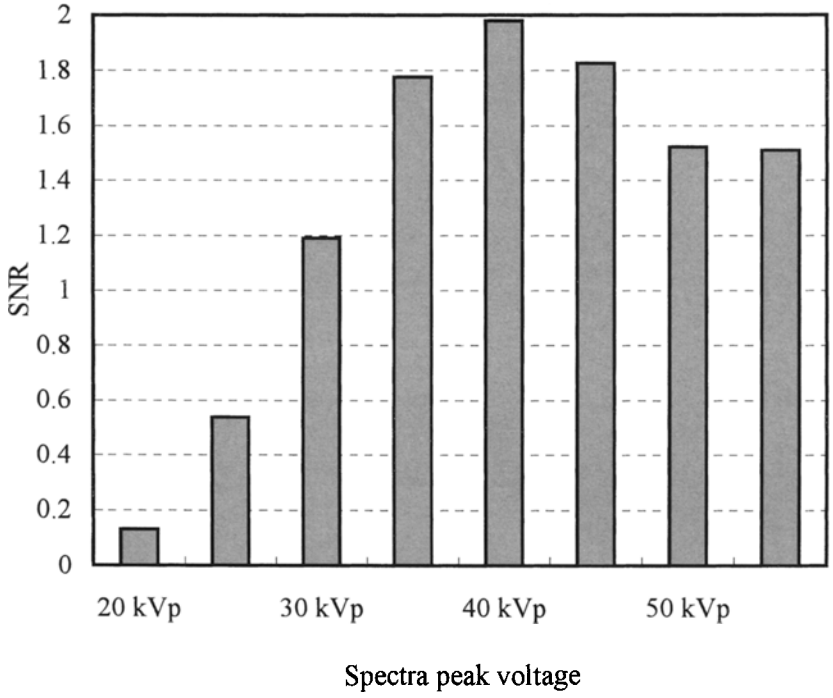

Fig 9. SNR versus X-ray tube voltage for dual screen measurement.

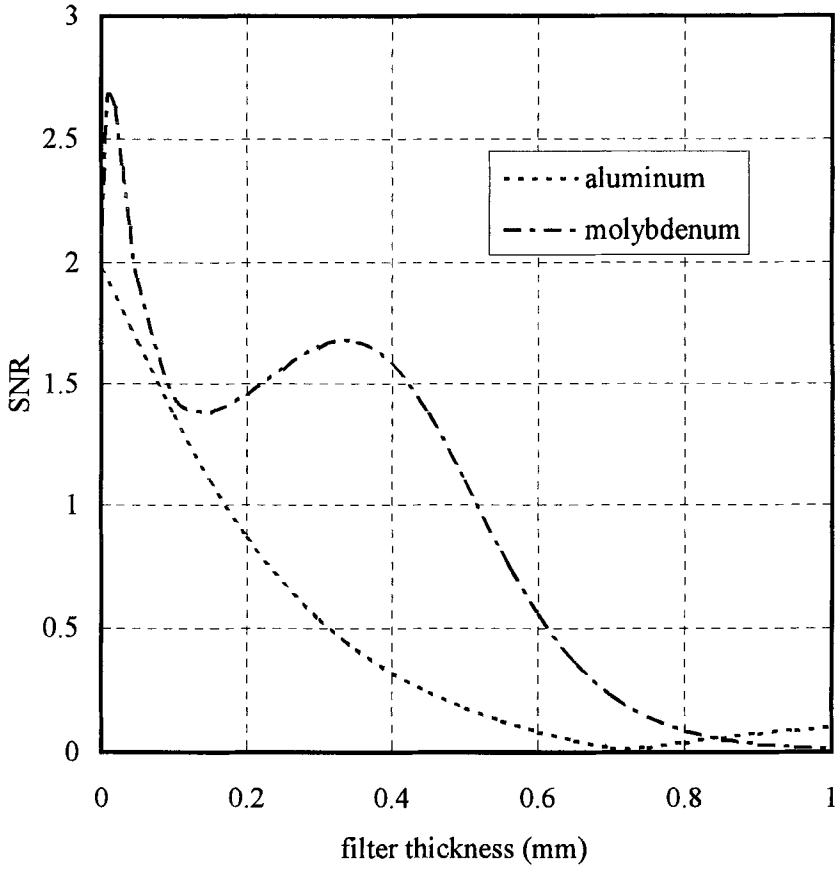

Fig 10. SNR versus filter thickness for two different prepatient filters in dual screen measurement.

any improvement at all. Filtration by molybdenum was much less efficient, requiring unreasonably large heat load to the tube for significant improvement, eg, from 13.2 to 15.9 with a heat loading factor of 53.3 by using 0.02 mm thick molybdenum to filter the low-kVp X-rays.

Dual Screen Method

The SNRs computed for the dual screen method are plotted as a function of kVp in Fig 9. The plot shows that the SNR peaks around 40 kVp (2.0), significantly higher than those at 35 and 45 kVp. Thus, proper kVp selection is more critical for the dual-screen method than for the SEH method.

The SNR computed for the dual-screen method is plotted as a function of the filter thickness in Fig 10 for aluminum and molybdenum. The plot shows that filtration by 0.01 mm of molybdenum produces highest SNR at 2.7, as compared to 2.0 obtained with unfiltered spectrum. This improvement can be achieved with a reasonably low tube loading factor of 10.3. The use of aluminum as the filter material, however, did not result in any SNR improvement.

Comparison of the Three Techniques

The SNRs obtained with the three tissue composition measurement techniques vary significantly with the kVp and prepatient filtration used. From the results of the SNR computations, it is obvious that the SEH method is an order of magnitude better than the dual kVp method, which, in turn, is an order of magnitude better than the dual screen method. By using the optimal kVp's and no prepatient filtration, the SNRs were computed to be 84.2, 13.2, and 2.0 for the SEH, dual kVp, and dual screen methods, respectively.

REFERENCES

1. Shaw de Paredes E: Radiographic breast anatomy: Radiologic signs of breast cancer, in Haus AG, Yaffe MJ (eds): Syllabus: A Categorical Course in Physics–Technical Aspects of Breast Imaging (ed 3). Oak Brook, IL, RSNA, 1994, pp 35-46
2. Yaffe MJ, Jennings R, Fahrig R, et al: X-ray spectral considerations for mammography, in Haus AG, Yaffe MJ (eds): Syllabus: A Categorical Course in Physics–Technical Aspects of Breast Imaging (ed 3). Oak Brook, IL, RSNA, 1994, pp 63-74
3. Byng JW, Boyd NF, Fishell E, et al: The quantitative analysis of mammographic densities. Phys Med Biol 39:1629-1638, 1994
4. Leinster SJ, Walsh PV, Whitehouse GH, et al: Factors associated with mammographic parenchymal patterns. Clin Raiol 39:252-256, 1988
5. Saftlas AF, Hoover RN, Brinton LA, et al: Mammographic parenchymal patterns as indicators of breast cancer risk. Cancer 67:2833-2838, 1991
6. Warner E, Lockwood G, Tritchler D: The risk of breast cancer associated with mammographic parenchymal patterns: A meta-analysis of the published literature to examine the effect of method of classification. Cancer Detect Prev 16:67-72, 1992
7. Byrne C, Schairer C, Wolfe J, et al: Mammographic features and breast cancer risk: effects with time, age, and menopause status. J Natl Cancer Inst 87:1622-1629, 1995
8. Boyd NF, Byng JW, Jong RA, et al: Quantitative classification of mammographic densities and breast cancer risk: Results from the Canadian National Breast Screening Study. J Natl Cancer Inst 87:670-675, 1995
9. Rowlands JA, Hunter DM, Araj N: X-ray imaging using amorphous selenium: A photoinduced discharge readout method for digital mammography. Med Phys 18:421-431, 1991
10. Yaffe MJ: Direct digital mammography using a scanned-slot CCD imaging system. Med Prog Technol 19:13-21, 1993
11. Karellas A, Harris LJ, D'Orsi CJ: Small field digital mammography with a 2048 × 2048 pixel charge coupled device. Radiology 177(P):288, 1990 (abstr)
12. Williams MB, Liu H, Fajardo LL, et al: Imaging properties of a prototype digital detector for full-breast mammography. Radiology 197(P):291, 1995 (abstr)
13. Shaw CC, Wang TP, Breitenstein DS, et al: A high resolution storage phosphor imaging system for mammographic imaging. Med Phys 22:997, 1995 (abstr)
14. Workman A, Cowen AR, Brettle DS: Physical evaluation of computed radiography as a mammographic x-ray imaging system. Brit J Radiol 67:988-996, 1994
15. Lehmann LA, Alvarez RE, Macovski A, et al: Generalized image combinations in dual kVp digital radiography. Med Phys 8:659-667, 1981
16. Gauntt DM, Barnes GT: X-ray tube potential, filtration, and detector considerations in dual-energy chest radiography. Med Phys 21:203-218, 1994
17. Cardinal HN, Fenster A: An accurate method for direct dual-energy calibration and decomposition. Med Phys 17:327-341, 1990
18. Johns PC, Drost DJ, Yaffe MJ, et al: Dual-energy mammography: Initial experimental results. Med Phys 12:297-304, 1985
19. Johns PC, Yaffe MJ: Theoretical optimization of dual-energy x-ray imaging with applications to mammography. Med Phys 12:289-296, 1985
20. Boone JM, Shaber GS, Tecotzky M: Dual-energy mammography: A detector analysis. Med Phys 17:665-675, 1990
21. Brettle DS, Cowen AR: Dual-energy digital mammography utilizing stimulated phosphor computed radiography. Phys Med Biol 39:1989-2004, 1994
22. Johns PC, Beauregard RM: Incorporation of scattered radiation into dual-energy radiologic theory and application to mammography. Med Phys 21:1455-1462, 1994

23. Gingold EL, Hasegawa BH: Systemic bias in basismaterial decomposition applied to quantitative dual-energy x-ray imaging. Med Phys 19:25-33, 1992

24. Moreau M, Holdsworth DW, Fenster A: Dual-energy x-ray imaging technique for in vitro tissue composition measurement. Med Phys 21:1807-1815, 1994

25. Nishitani H, Umezu Y, Kazuhisa O, et al: Dual-energy projection radiography using condeser x-ray generator and digital radiography aparatus. Radiology 161:533-535, 1986

26. Ishigaki T, Sadayuki S, Yoshimi H, et al: One-shot dual-energy subtraction imaging. Radiology 161:271-273, 1986

27. Stewart BK, Huang HK: Single-exposure dual-energy computed radiography. Med Phys 17:866-875, 1990

28. Shaw CC, Gur D: Comparison of three different techniques for dual-energy subtraction imaging in digital radiography: A signal-to-noise analysis. J Digit Imaging 5:262-270, 1992

29. White DR, Martin RJ, Darlison R: Epoxy resin based tissue substitutes. Brit J Radiol 50:814-821, 1977

30. Nishikawa RM, Yaffe MJ: Model of the spatial-frequency-dependent DQE of phosphor screens. Med Phys 17:894-904, 1990

31. Fewell TR, Shuping RE: Handbook of Mammographic X-ray Spectra. Rockville, MD, U.S. Department of Health, Education, and Welfare, 1978 (DHEW Publication No. (FDA) 79-8071)

32. Storm E, Israel HI: Photon cross sections from 1 keV to 100 MeV for elements Z = 1 to Z = 100,* in Nuclear Data Tables. New York, NY, Academic, 1970, A7:565-681

33. Johns HE, Cunningham JR: The Physics of Radiology. Springfield, IL, Thomas, 1983

34. Fuji Imaging Plates ST-III and HR-III and Fuji CR Film Types 633 and 780 for Computed Radiography. Tokyo, Japan, Fuji Photo Film Co, Ltd.